Adsorption (2008) 14: 719–726
DOI 10.1007/s10450-008-9109-x

Influence of quantum effects on the mechanism of adsorption and phase diagram of rare gases in carbon nanotubes

L. Firlej · B. Kuchta

Received: 30 April 2007 / Revised: 5 November 2007 / Accepted: 8 February 2008 / Published online: 4 March 2008

Abstract We present results of grand canonical Monte Carlo simulations of rare gases (He, Ne, Ar, Kr and Xe) adsorption in carbon nanotubes. The interaction model includes both quantum effects (via effective Feymann-Hibbs potential) and the atomic roughness of the tube. We show that the quantum contribution to interactions does not suppress the energetic corrugation of carbon nanotube but decreases only its average strength. In the case of Ne, the phase diagram and, in particular, the melting temperature for layers adsorbed on and within an individual tube does not depend on tube chirality. However, the structure of layers adsorbed on outer surface of the tube is strongly related to the atomic structure of the underlying tube.

Keywords Molecular modeling · Adsorption mechanism · Quantum effects · Surface heterogeneity · Phase diagram

1 Introduction

At the atomic level, the adsorbing surfaces are always heterogeneous. However, in analysis of physical properties of the adsorbate, the atomic roughness of the adsorbent is very often neglected. There are at least two reasons for that. First, in real macroscopic objects structural heterogeneity of the adsorbing surfaces is mainly determined by mesoscopic imperfections (defects, domain structure, grain boundaries etc.). Their sizes are several orders of magnitude larger than the dimensions of atoms building the surface and in many cases it is adsorption on defects that determines the general features of adsorption, in particular the shape of the adsorption isotherm. Second, even when the substrate is crystallographically perfect, the energetic heterogeneity of the substrate due to its atomic structure persists but it usually makes less than 1% of the total energy of the system. Thus, at high temperature it becomes negligible with respect to the thermal energy of the adsorbed atoms and the energy barriers between the adsorption sites that are due to the atomic roughness of the substrate can be easily crossed. Some questions concerning the role of the surface heterogeneity, initially discussed by Bojan and Steele (1988) for flat adsorbents, have been recently revisited for heterogeneous nanoporous materials (Maddox et al. 1997; Vuong and Monson 1998; He and Seaton 2003; Kuchta et al. 2004; Ravikovitch et al. 2006; Ravikovitch and Neimark 2006; Coasne et al. 2006; Kuchta et al. 2007).

The situation changes when adsorption occurs at low temperature. When the amplitude of thermal movements of gas atoms become comparable to (or smaller than) the atomic roughness of the substrate, the system may be trapped in a variety of long-living metastable states which have distinctly different structures. As the process of adsorption is a result of a delicate balance between adhesive (gas–surface) and cohesive (gas–gas) forces, the knowledge of details of the potential energy landscape becomes essential. Every attempt to describe the adsorption mechanism at the microscopic level should take into account both aspects of the surface roughness: geometric one, resulting from spatial distribution of the adsorption sites and energetic one, related to their non-uniform strength.

L. Firlej
Laboratoire des Colloïdes, Verres et Nanomatériaux (LCVN), Université Montpellier II, 34095 Montpellier, France

B. Kuchta (✉)
Laboratoire des Matériaux Divises, Revêtement, Electrocéramiques (MADIREL), Université de Provence, Centre de Saint-Jérôme, 13397 Marseille, France
e-mail: kuchta@up.univ-mrs.fr

In the case of rare gases adsorption in nanoporous materials, because of the small mass of adsorbate and strong confinement, quantum effects are expected to affect significantly the adsorption mechanism (Wang and Johnson 1997, 1999; Shi and Johnson 2003; Tanaka et al. 2005; Kowalczyk et al. 2005). It is commonly agreed that at low temperatures zero point motion energy of gas atoms is larger than the corrugation component of their interaction with the substrate. Using this argument, in many simulations of low temperature adsorption of quantum gases the substrates have been represented as smooth surfaces and their real atomic structure usually has been neglected.

In this paper we present detailed study of the influence of quantum effects on effective substrate corrugation, mechanism of adsorption and phase diagrams of rare gases adsorbed at low temperature within individual carbon nanotubes (NT). To verify the validity of the tube wall approximation by a smooth cylinder we calculated the effective energetic corrugation for gases adsorption on both external and internal surfaces of carbon nanotubes of various radii and chirality, and on graphite surface. To take into account the quantum effects, both gas-gas and gas-carbon nanotube interactions have been modeled by Feymann-Hibbs (FH) effective potential. The results have been compared to those obtained using classic LJ model of interaction (Firlej and Kuchta 2005). The calculations are performed for a large variety of tubes diameters and chiralities.

2 Model of interaction

To take into account the quantum effects, we performed all simulations using the Feymann-Hibbs (FH) effective potential (Feymann and Hibbs 1965; Feymann 1972). In this approximation, the quantum fluid is represented by a Gaussian wave packet of width $h/(24\pi m k_B T)^{1/2}$, so that FH effective potential is an average of classical Lennard-Jones (LJ) potential over the wave packet. Here m is a mass of fluid atom. According to Sese (Sese 1994, 1995), for a good approximation of rigorous path integral Monte Carlo simulations of fluid it is sufficient to cut this Gaussian FH potential at the second order terms. As a result, the final formula for calculation of the fluid-fluid interaction is given as

$$V_{\mathrm{FH}}^{\mathrm{ff}}(r) = V_{\mathrm{LJ}}^{\mathrm{ff}}(r) + \left(\frac{\beta\hbar^2}{24\mu_m}\right)\left[\frac{d^2}{dr^2}V_{\mathrm{LJ}}^{\mathrm{ff}}(r) + \frac{2}{r}\frac{d}{dr}V_{\mathrm{LJ}}^{\mathrm{ff}}(r)\right]$$

where

$$V_{\mathrm{LJ}}^{\mathrm{ff}}(r) = 4\varepsilon^{\mathrm{ff}}\left[\left(\frac{\sigma^{\mathrm{ff}}}{r}\right)^{12} - \left(\frac{\sigma^{\mathrm{ff}}}{r}\right)^{6}\right]$$

$\mu_m = m/2$ is the reduced mass of interacting pair of fluid molecules, $\beta = (k_B T)^{-1}$, $\varepsilon^{\mathrm{ff}}$ and σ^{ff} are the LJ parameters of fluid. We used the values of $\varepsilon^{\mathrm{ff}}$ and σ^{ff} as reported by Steele (Steele 1978).

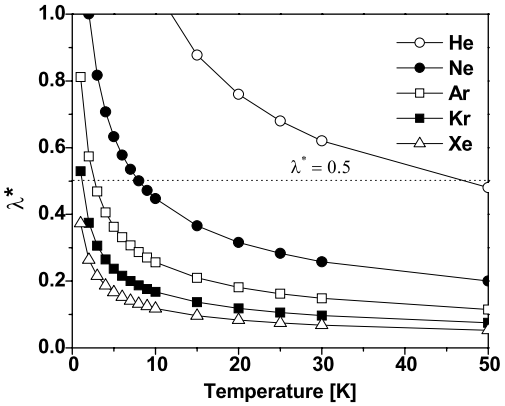

Fig. 1 Reduced thermal wavelength $\lambda^* = h/(2\pi m k_B T \sigma_{\mathrm{ff}}^2)^{1/2}$ for rare gases as a function of temperature. According to Sese, Feymann-Hibbs approximation of quantum effects may be applied in the temperature range when $\lambda^* < 0.5$

According to Sese calculations, the second-order FH truncated potential can be used instead of rigorous path integral Monte Carlo calculation when the reduced de Broglie thermal wavelength $\lambda^* = h/(2\pi m k_B T \sigma_{\mathrm{ff}}^2)^{1/2} \leq 0.5$. Figure 1 shows the variation of λ^* value with temperature for all rare gases. It is clear, that the FH effective potential can not be used for calculation of helium properties, as far as $T < 50$ K. As the experimental works (Teizer et al. 1999, 2000; Lasjaunias et al. 2003, 2002) showed that He totally desorbs from NT samples at temperature $T \sim 24$ K, it means that the He adsorption in NT must be exactly considered via path integral calculations. In the case of Ne, the limiting temperature is of the order ~8 K. Consequently, we used FH effective potential to simulate the phase diagram of Ne adsorbed within and on isolated carbon nanotubes of different chiralities. For Ar, Kr and Xe the limiting temperature is lower than 3D boiling He temperature so the FH approximation can be used in the whole temperature range starting from $T = 3$ K.

The fluid-nanotube wall interaction $V_{\mathrm{FH}}^{\mathrm{fw}}$ was computed using a pair-wise summation of fluid-carbon potential in the cut-off sphere of the radius of 15 Å. In this case, as we considered that the carbon atoms in NT wall are linked rigidly, we used $\mu_m = m$ for the quantum interaction between fluid and carbon atoms instead of $\mu_m = m/2$ applied for fluid-fluid potential. The values $\varepsilon^{\mathrm{fw}}$ and σ^{fw} of LJ potential were obtained from Lorentz-Berthelot mixing rules, taking $\varepsilon_{\mathrm{CC}} = 28.0$ K, $\sigma_{\mathrm{CC}} = 3.4$ Å (Steele 1978). To account for the structural (atomic) roughness of the tube neither axial nor azimuthal smoothing of the potential was done.

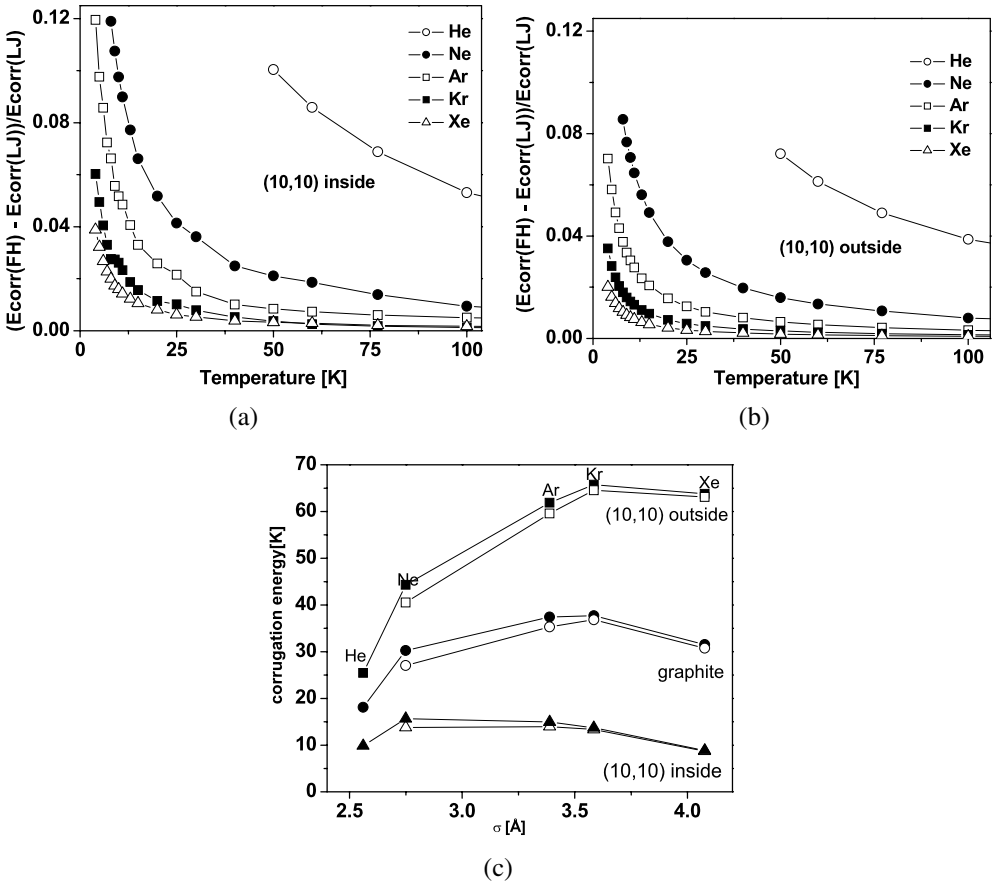

Fig. 2 Relative (with respect to classic Lennard-Jones, LJ) contribution of quantum correction to the interaction potential for rare gases adsorbed on (**a**) inside, (**b**) outside the (10,10) NT carbon nanotube. (**c**) Corrugation of graphite and (10,10) NT as a function of σ^{ff} potential parameter. *Open symbols* correspond to Feymann-Hibbs (FH) model of interaction ($T = 10$ K), *full symbols*—to LJ model

3 Results

To characterize the energetic roughness of carbon nanotubes (and graphite) we defined two parameters: the corrugation energy and the saddle energy. The corrugation energy is a maximal energy barrier for atomic moves on the substrate; similarly, the saddle energy is the lowest energy barrier for such moves. In the case of graphite these values correspond to a difference between the minimal energy of atom adsorbed above the center of hexagonal lattice and, respectively above carbon atom or carbon-carbon bond. In the case of carbon nanotubes, the graphite sheet is not planar and identification of saddle energy, which depends on both tube radius and chirality, is more complex.

Figure 2 shows the contribution of quantum FH correction to the corrugation energy for rare gases adsorbed on isolated (10,10) NT, on its inner (Fig. 2a) and outer (Fig. 2b) surface. The armchair (10,10) carbon nanotube is an example, widely used in simulation literature, of the family of tubes of the diameter 14–17 Å, the most frequently obtained in standard synthesis procedure. Even at temperature as high as 50 K, the quantum correction for He constitutes ∼10% of the total corrugation and decreases very slowly with temperature. For Ar, Xe and Kr, at helium temperatures, this correction is only of the order of 3%. This is clearly seen on Fig. 2c, where the absolute values of corrugation energy for all gases are given as a function of LJ σ^{ff} potential parameter, which is almost equal to the gas atom size.

The corrugation is the largest and almost the same for Ar, Kr and Xe. For these gases, and for the tube diameter of ∼7.5 A, the mismatch between fluid-fluid equilibrium distance and the graphite unit cell vectors is the lowest, so the adsorbed atoms experiences the highest barriers for moving from one adsorption site to an other.

Figure 3 presents detailed comparison of quantum contribution to the corrugation energy in a case of Ne adsorbed on graphite and on isolated (10,10) and (20,20) carbon nanotubes. The fraction of quantum correction to the corrugation energy (Fig. 3a) is only slightly dependent on the tube curvature and is comparable to the corrugation of graphite. At $T = 8$ K, the lowest temperature for which the FH approximation can be applied, it constitutes 20% of the LJ value and decreases with temperature to <1% at $T = 100$ K. The quantum correction never suppresses the energetic cor-

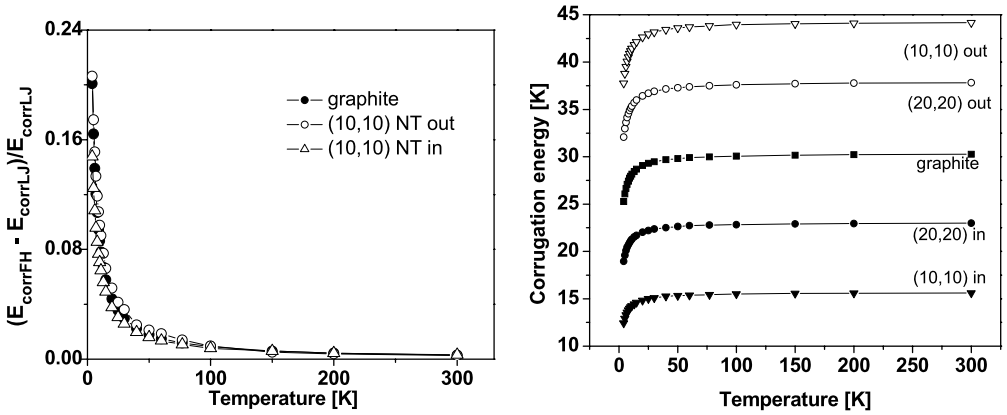

Fig. 3 (**a**) Relative (with respect to classical LJ) contribution of quantum correction to the interaction potential for Ne adsorbed on of carbon surfaces: inside and outside (10,10) NT and on graphene sheet. (**b**) Absolute value of corrugation of different carbon surfaces

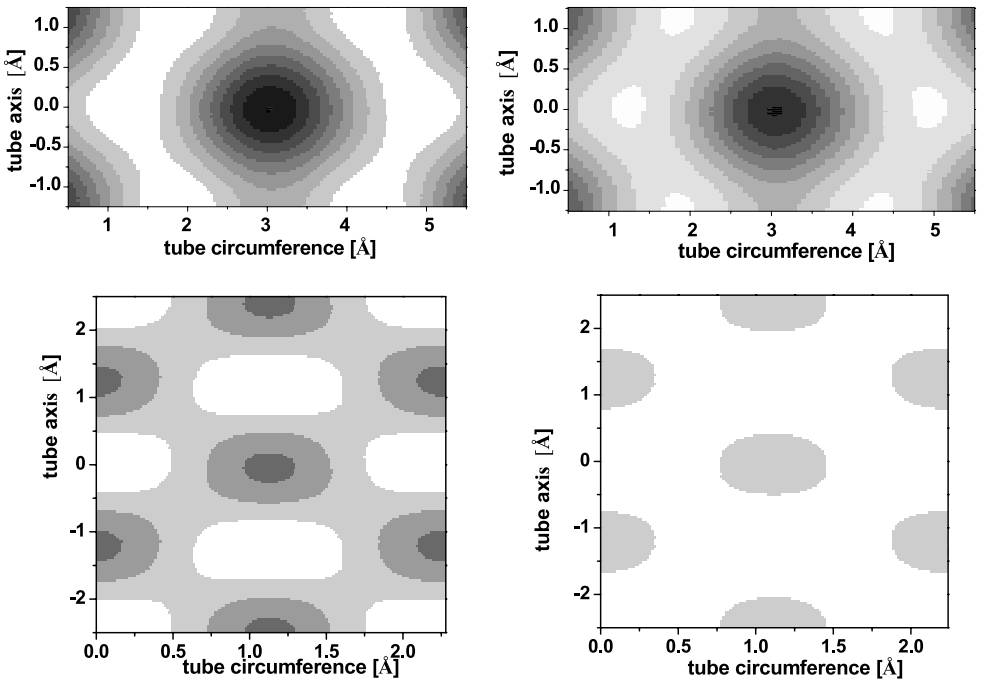

Fig. 4 Energy landscape outside (*upper graphs*) and inside (*lower graphs*) (10,10) NT: adsorption of Ne. *Left graphs*: LJ model of interaction. *Right graphs*: FH effective model ($T = 8$ K)

rugation of the wall (Fig. 2b). F.ex. for (10,10) tube at $T = 8$ K the corrugation energy is $E_{\text{corr}} = 37$ K. So, at low temperature atomic corrugation of the wall is still an important factor that can localize fluid atoms in strongly adsorbing sites and influence the mechanism of melting of the adsorbed layers.

Figure 4 gives a comparison of energy landscape seen by Ne atom adsorbed outside and inside (10,10) carbon nanotube when either LJ or FH model on interaction is used. Adding quantum correction to classical LJ potential model does not change a lot the energy distribution outside the tube; the quasi-1D low energy path appearing in the direction parallel to the tube axis is slightly smear out, but still conserved. On the contrary, dramatic changes are observed inside the tube. In LJ approximation corrugation energy is of the order of 20 K, twice as high as thermal energy at $T = 8$ K, and strongly localizes the adsorbed atoms in attractive sites and on low energy paths between them. In FH model the corrugation is smeared out and becomes of the same order of magnitude that the thermal energy. The adsorbed atoms move around the confined volume nearly freely, regardless the wall structure.

The energetic roughness of a carbon nanotube is obviously related to its radius and type of chirality. Figure 5a shows the variation of both corrugation and saddle energy for Ne adsorbed inside and outside armchair type (n,n) nan-

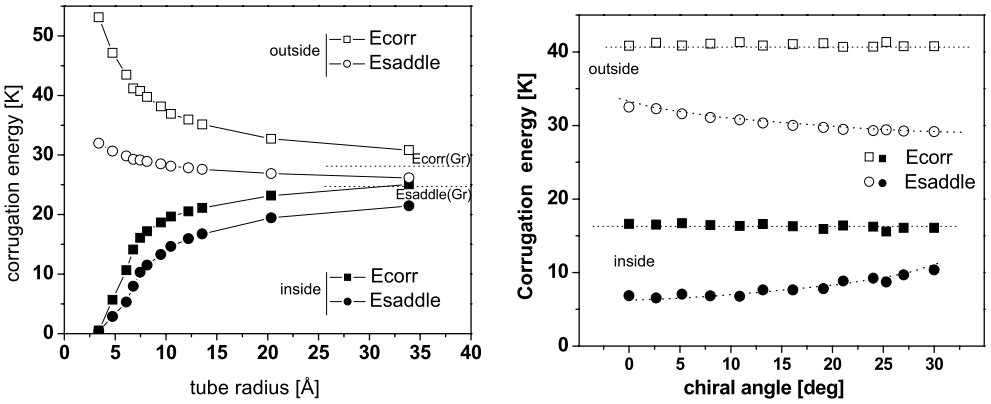

Fig. 5 (**a**) Corrugation and saddle energy of armchair-type NT as a function of tube radius. (**b**) Corrugation and saddle energy of NT of the radius $R \sim 7.4$ Å as a function of chiral angle

otubes, as a function of tube radius. When the radius increases, both energies tend exponentially to the values characteristic for flat graphite surface. Interestingly, for the nanotubes (5,5) both energies decrease to zero for adsorption inside the tube. It means that the smallest carbon nanotubes, of the same diameter as C_{60} molecule, can be considered as a realization of energetically smooth nanopores for Ne adsorption. For larger gases, the pore can be considered as smooth for larger tube diameters; f.ex. for Xe adsorption, the tube (7,7) is still energetically smooth. The nanotubes of small diameters are thus the materials that may allow an experimental realization on 1D confinement of atoms, without energetic or structural constraints.

Figure 5b shows the variation of corrugation and saddle energy as a function of chiral angle. Here the tube radius has been kept constant, $R \sim 7.5$ Å. The corrugation energy is clearly chirality independent. The saddle corrugation depends on chirality in different way inside and outside the tube. Outside the tube, the saddle corrugation is minimal for armchair type tubes (chiral angle $\alpha = 30°$). A quasi-1d lines of low energy barriers for atom moves appear on the tube surface, parallel to the tube axis. When the chiral angle decreases, the low energy lines rotates and for $\alpha = 0°$ (zig-zag tubes) they form a network intersecting at the angle of 60°. Such intricate configuration is energetically less favorable and the saddle energy increases. Inside the tube the situation is reversed: the low energy lines form lines around tube circumference and passing above the C–C bonds for zig-zag type nanotubes, $\alpha = 0°$. When the chiral angle increases the lines deform, intersect and finally for armchair type tubes the network of lines intersecting at the angle of 120° appears. The difference of saddle energy between armchair and zig-zag nanotubes is not high, ∼4 K for both inner and outer surface of the tube. Therefore, the chirality should not affect much the temperature of melting of the adsorbed layers but could modify their low temperature structure.

To verify this hypothesis, we have performed grand canonical Monte Carlo simulations of Ne adsorption on 3 isolated, open-ended carbon nanotubes of different chiralities: armchair (11,11) NT (chiral angle $\alpha = 30°$, $R = 7.46$ Å), zig-zag (18,0) NT ($\alpha = 0°$, $R = 7.05$ Å) and chiral (16,4) NT ($\alpha = 10.89°$, $R = 7.18$ Å). The tubes have been chosen to represent the whole range of chiralities, from 0° to 30° and to have comparable diameters. Figure 6 shows the energy surface (inner and outer) for all the tubes, calculated using FH effective potential, at $T = 8$ K. Each simulation has been performed on an individual tube, placed at the center of MC box, with periodic boundary conditions in the tube axis direction. The calculations of phase diagram have been performed for the temperatures $8\ \text{K} < T < 80\ \text{K}$ and pressures $10^{-13} < p < 10^{3}$ mbar without crossing, at each temperature, the saturation pressure p_0 of 3D gas.

The phase diagram of Ne adsorbed on carbon nanotubes of comparable radius is chirality independent. As an example, Fig. 7 shows the phase diagram for adsorption on (11,11) NT. The adsorption region is bordered by two lines: the lower one indicates the (p, T) values for which Ne totally desorbs from the tube and the upper one (noted p_0) is the line of saturation pressure of 3D gas. The line of capillary condensation (CC) is at the same position as the line of monolayer formation on the outer surface of the tube. The solid vertical line shows the limit of FH effective potential applicability ($T = 8$ K); the dashed line marks the melting temperature of 3D solid. The structure of phase diagram and the details of mechanism of melting will be discussed elsewhere. Here we focus only on the relation between wall roughness and structures of the adsorbed monolayer.

Figure 8 shows the structure of the monolayer adsorbed on (11,11) and (18,0) carbon nanotubes, in the solid and liquid phase. For the armchair (11,11) tube, at low temperature the fluid atoms are confined near the strong adsorption sites

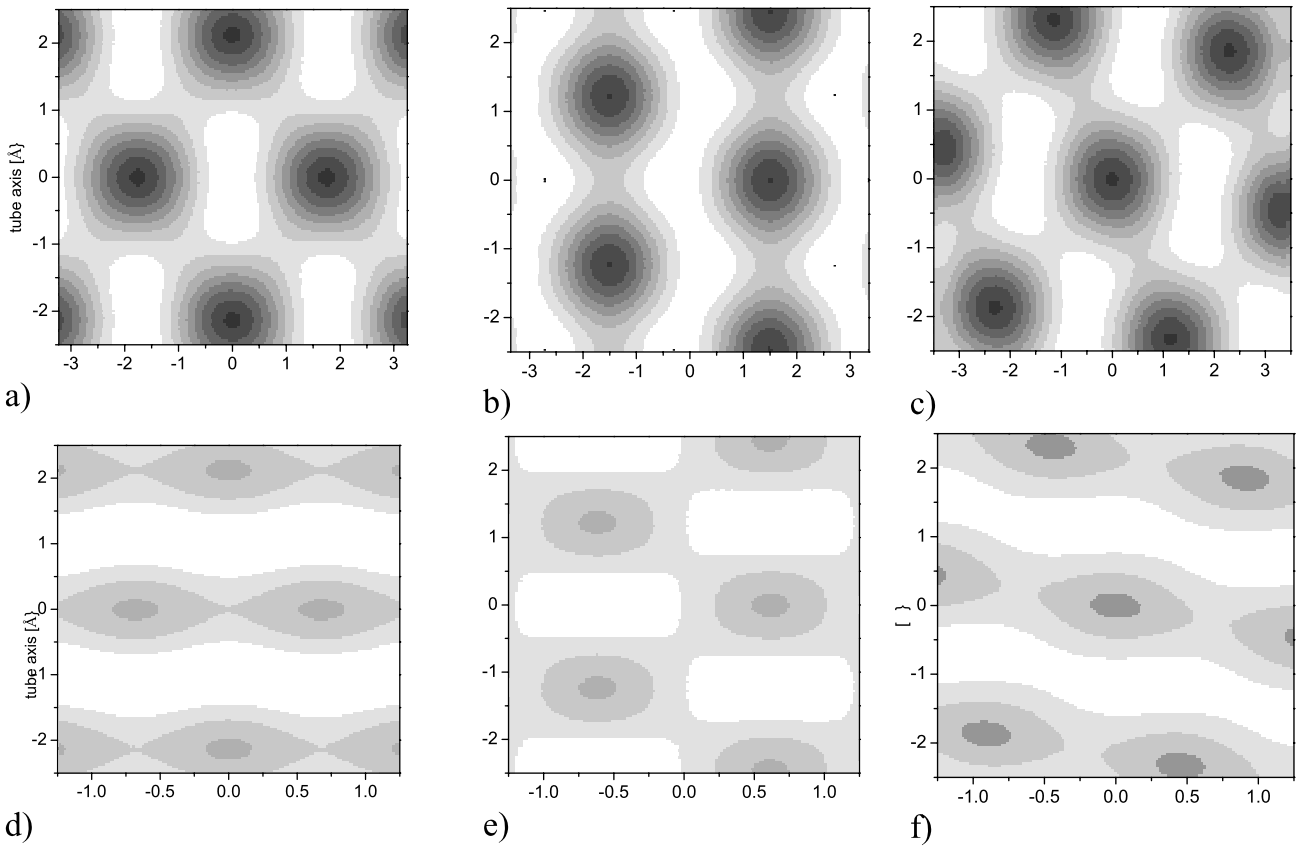

Fig. 6 Energy landscape outside (*upper graphs*) and inside (*lower graphs*) carbon nanotubes of comparable diameter (∼7 Å) but different chiralities: zigzag (18,0) (**a**, **d**), armchair (11,11) (**b**, **e**), chiral (16,4) (**c**, **f**)

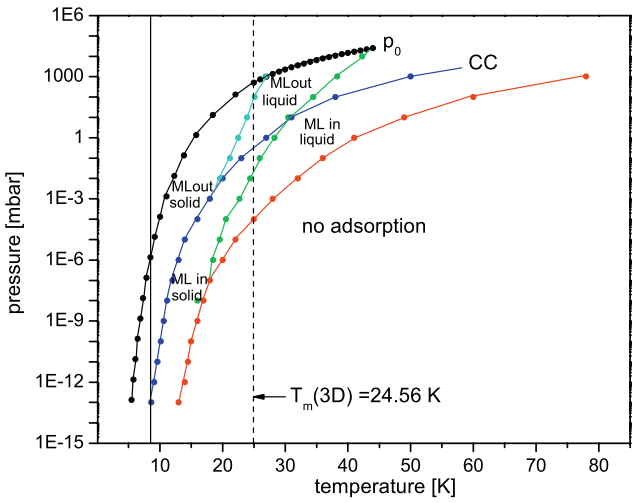

Fig. 7 Phase diagram of Ne adsorbed on and within an isolated (11,11) carbon nanotube

(the carbon hexagons centers) and form distorted triangular lattice. Because of the incommensurability of both (nanotube corrugation and neon) lattices at relatively low pressures ($p \sim 10^{-10}$ mbar) a modulation of the structure density appears. Increasing pressure at low temperature localizes atoms even more; the modulation of density is followed by formation of 2D domains that structures and orientations with respect to the carbon wall vary. When the thermal energy increases and becomes comparable to saddle and than corrugation energy, the fluid atoms start to move between the adsorption sites along the minimal energy lines, parallel to the tube axis. This motion is strongly correlated and the instantaneous configurations preserve their solid-phase structure. Even after the melting the preferential direction of atoms motion is conserved (Fig. 8c) and becomes totally disordered only at high temperature, far beyond melting transition, when a part of monolayer is already evaporated and there is more room for atoms to move. At the same time, as the thermal energy of atoms is already larger than corrugation energy, the exploration of the whole energy surface is possible.

The monolayer adsorbed on (18,0) is not anchored on the substrate even at lowest temperature and pressure (Fig. 8b). It may be due to the larger misfit of monolayer and substrate corrugation lattices, forcing the fluid atoms to find the equilibrium positions on the lines of lowest fluid-wall energy. For the same reason, in the liquid phase the totally

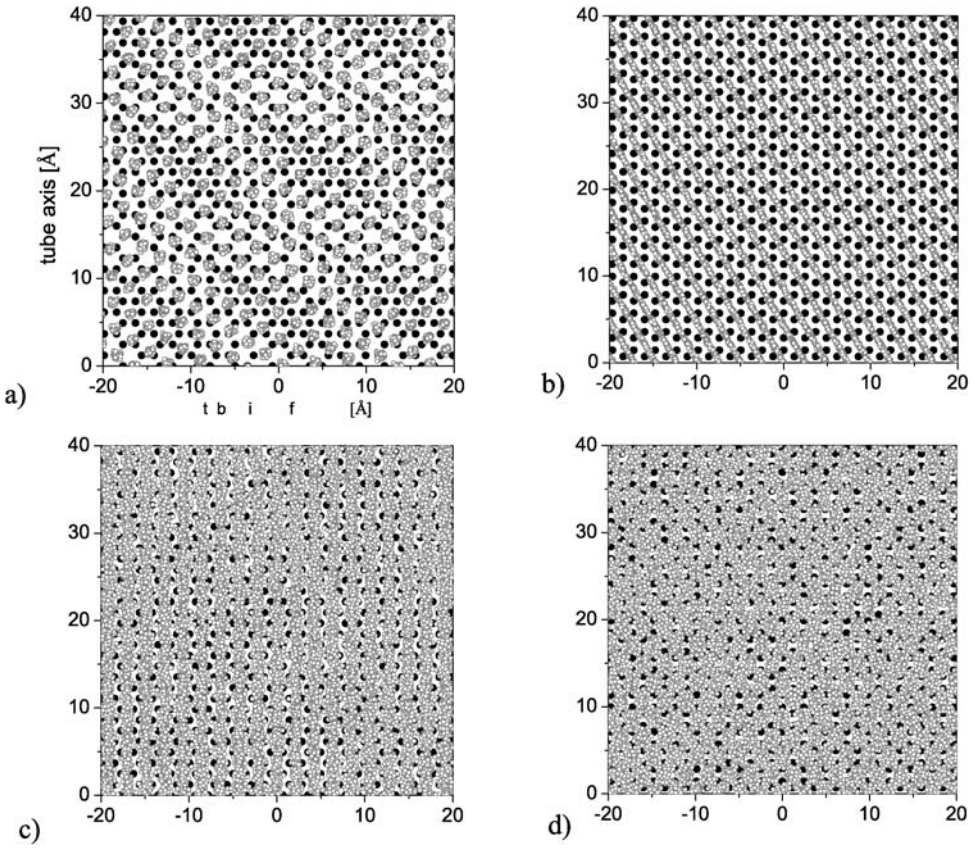

Fig. 8 Structure of the first layer of Ne adsorbed on the outer surface of carbon nanotubes in solid (*upper graphs*) and liquid (*lower phase*) phase. Closed black symbols are carbons forming nanotubes; open gray symbols denote Ne atoms: (**a**, **c**) armchair (11,11) tube, (**b**, **d**) zigzag (18,0) tube

disordered structure appears directly at the melting transition, although some reminders of the tube corrugation are still visible (Fig. 8d).

4 Conclusions

In summary, we have shown that adding quantum correction to the classical Lennard-Jones model of the interaction does not change qualitatively the overall picture of energy landscape for rare gases adsorption on carbon nanotubes. As far as the adsorption on the outer tube surface is concerned, the atomic structure of the wall always leads to its energetic heterogeneity and distribution of adsorption sites. Depending on the tube chirality and the mismatch between fluid-fluid equilibrium distance and the distance between the adjacent adsorption sites, a variety of monolayer structures can be formed. Consequently, melting of solid monolayer into totally disordered liquid may be preceded by an activation of a cooperative quasi-1D movement of adsorbed atoms along specific low energy path between adsorption sites.

On the contrary, the presence of quantum term changes dramatically the energetic structure in the case of adsorption on the internal surface of carbon nanotubes. The energy distribution is significantly smeared out and, for the tubes of diameter smaller than 10 Å, the internal surface of carbon nanotubes can be considered as energetically smooth for rare gases adsorption, despite the discrete, atomic structure of the tube wall.

References

Bojan, M.J., Steele, W.A.: Computer simulation of physisorption on a heterogeneous surface. Surf. Sc. Lett. **199**, L395–L402 (1988)

Coasne, B., Galarneau, A., Di Renzo, F., Pellenq, R.J.M.: Gas adsorption in mesoporous templated silicas: MCM-41, MCM-48 and SBA-15. Langmuir **22**, 11097–11105 (2006)

Feymann, R.P.: Statistical Mechanics. Benjamin, New York (1972)

Feymann, R.P., Hibbs, A.: Quantum Mechanics and Path Integrals. McGraw-Hill, New York (1965)

Firlej, L., Kuchta, B.: Low temperature phases of rare gases adsorbed on single wall carbon nanotubes. J. Low Temp. Phys. **139**, 599 (2005)

He, Y.F., Seaton, N.A.: Experimental and computer simulation studies of the adsorption of ethane, carbon dioxide, and their binary mixtures in MCM-41. Langmuir **19**, 10132–10138 (2003)

Kowalczyk, P., Tanaka, H., Holyst, R., Kaneko, K., Ohmori, T., Miyamoto, J.: Storage of hydrogen at 303 K in graphite slit-like pores from grand canonical Monte Carlo simulation. J. Phys. Chem. B **109**, 17174 (2005)

Kuchta, B., Llewellyn, P., Denoyel, R., Firlej, L.: Modeling of pore wall amorphous structures: influence of wall heterogeneity on the mechanism of adsorption. Krypton and argon adsorption in MCM-41 pore model. Colloids Surf. A: Physicochem. Eng. Asp. **241**, 137–142 (2004)

Kuchta, B., Firlej, L., Boulet, P., Marzec, M.: Adsorption in cylindrical pores: mixed lattice-site/off-site Monte Carlo simulations in pores with heterogeneous wall structure. Appl. Surf. Sci. (2007, in press)

Lasjaunias, J.C., Biljakovic, K., Benes, Z., Fischer, J.E., Monceau, P.: Low temperature specific heat of single-wall carbon nanotube. Phys. Rev. B **65**, 113409–113412 (2002)

Lasjaunias, J.C., Biljakovic, K., Sauvajol, J.L., Monceau, P.: Evidence of 1D behavior of He4 confined within carbon nanotube bundles? Phys. Rev. Lett. **91**, 25901–25904 (2003)

Maddox, M.W., Olivier, J.P., Gubbins, K.E.: Characterization of MCM-41 using molecular simulation: heterogeneity effect. Langmuir **13**, 1737–1745 (1997)

Ravikovitch, P.I., Neimark, A.V.: Density functional theory model of adsorption on amorphous and microporous silica materials. Langmuir **22**, 11171–11176 (2006)

Ravikovitch, P.I., Vishnyakov, A., Neimark, A.V., Ribero Carrott, M.M.L., Russo, P.A., Carrot, P.J.: Characterization of microporous materials from nitrogen and toluene adsorption: experiment and modeling. Langmuir **22**, 513–516 (2006)

Sese, L.M.: Study of the Feymann-Hibbs effective potential against the path integral formalism for Monte Carlo simulations of quantum many-body Lennard-Jonnes systems. Mol. Phys. **81**, 1297–1312 (1994)

Sese, L.M.: Feymann-Hibbs potentials and path integrals formalism for quantum Lennard-Jonnes systems: theory and Monte Carlo simulations. Mol. Phys. **85**, 931–947 (1995)

Shi, W., Johnson, J.K.: Gas adsorption on heterogeneous single-walled carbon nanotube bundles. Phys. Rev. Lett. **91**, 015504 (2003)

Steele, W.A.: Interaction of rare-gas atoms with graphitized carbon-black. J. Phys. Chem. **82**, 817–821 (1978)

Tanaka, H., Kanoh, H., Yudasaka, M., Iijima, S., Kaneko, K.: Quantum effects on hydrogen isotope adsorption on single-wall carbon nanohorns. J. Am. Chem. Soc. **127**, 7511 (2005)

Teizer, W., Hallock, R.B., Dujardin, E., Ebbesen, T.W.: He-4 desorption from single wall carbon nanotube bundles: a one-dimensional adsorbate. Phys. Rev. Lett. **82**, 5305–5308 (1999)

Teizer, W., Hallock, R.B., Dujardin, E., Ebbesen, T.W.: Erratum: 4He desorption from single wall carbon nanotube bundles: a one-dimensional adsorbate [Phys. Rev. Lett. **82**, 5305 (1999)]. Phys. Rev. Lett. **84**, 1844–1845 (2000)

Vuong, T.Y.F., Monson, P.A.: Surface roughness effects in molecular models of adsorption in heterogeneous porous solids. Langmuir **14**, 4880–4886 (1998)

Wang, Q., Johnson, J.K.: Phase equilibrium of quantum fluids from simulation: hydrogen and neon. Fluid Phase Equilib. **132**, 93–116 (1997)

Wang, Q., Johnson, J.K.: Molecular simulation of hydrogen adsorption in single-walled carbon nanotubes and idealized carbon slit pores. J. Chem. Phys. **110**, 577–586 (1999)